Published in final edited form as:
Cancer Res. 2009 February 1; 69(3): 967–975. doi:10.1158/0008-5472.CAN-08-2307.

Role of VDR in anti-proliferative effects of calcitriol in tumor-derived endothelial cells and tumor angiogenesis *in vivo*

Ivy Chung[1], **Guangzhou Han**[1], **Mukund Seshadri**[2], **Bryan M. Gillard**[1], **Wei-dong Yu**[1], **Barbara A. Foster**[1], **Donald L. Trump**[3], and **Candace S. Johnson**[1]

[1]Department of Pharmacology and Therapeutics, Roswell Park Cancer Institute, Buffalo, NY 14263

[2]Department of Cancer Biology, Roswell Park Cancer Institute, Buffalo, NY 14263

[3]Department of Medicine, Roswell Park Cancer Institute, Buffalo, NY 14263

Abstract

Calcitriol (1, 25-dihydroxycholecalciferol), the major active form of vitamin D, is anti-proliferative in tumor cells and tumor-derived endothelial cells (TDEC). These actions of calcitriol are mediated at least in part by vitamin D receptor (VDR), which is expressed in many tissues including endothelial cells. To investigate the role of VDR in calcitriol effects on tumor vasculature, we established TRAMP-2 tumors subcutaneously into either VDR wild type (WT) or knockout (KO) mice. Within 30 days post inoculation, tumors in KO mice were larger than those in WT ($P<0.001$). TDEC from WT expressed VDR and were able to transactivate a reporter gene whereas TDEC from KO mice were not. Treatment with calcitriol resulted in growth inhibition in TDEC expressing VDR. However, TDEC from KO mice were relatively resistant, suggesting that calcitriol-mediated growth inhibition on TDEC is VDR-dependent. Further analysis of the TRAMP-C2 tumor sections revealed that the vessels in KO mice were enlarged and had less pericyte coverage compared to WT ($P<0.001$). Contrast-enhanced MRI demonstrated an increase in vascular volume of TRAMP tumors grown in VDR KO mice compared to WT mice ($P<0.001$) and FITC-dextran permeability assay suggested a higher extent of vascular leakage in tumors from KO mice. Using ELISA and Western blot analysis, there was an increase of HIF-1 alpha, VEGF, Ang1 and PDGF-BB levels observed in tumors from KO mice. These results indicate that calcitriol-mediated anti-proliferative effects on TDEC are VDR dependent and loss of VDR can lead to abnormal tumor angiogenesis.

Keywords

vitamin D receptor knockout mice; tumor angiogenesis; tumor-derived endothelial cells

Introduction

Calcitriol has effects on multiple tissues by regulating cell proliferation, differentiation and apoptosis (1, 2). Calcitriol has profound anti-tumor activity in many *in vitro* and *in vivo* human and murine tumor models, including leukemia (3), squamous cell carcinoma (4), prostate (5), breast (6), and colon cancer (7). Calcitriol has anti-proliferative effects not only on malignant epithelial cells (2), but also on endothelial cells freshly isolated from tumors [tumor-derived endothelial cells (TDEC)] (8, 9). Treatment with calcitriol promotes G_0-G_1

Requests for reprints: Candace S. Johnson, Department of Pharmacology and Therapeutics, Roswell Park Cancer Institute, Elm and Carlton Streets, Buffalo NY 14263. Tel: 716-845-8300; Fax: 716-845-1258; e-mail: Candace.Johnson@roswellpark.org.

cell cycle arrest and induces apoptosis in TDEC (9, 10). The growth inhibition observed in TDEC is accompanied by modulation of cell cycle proteins (p21 and p27), down-regulation of survival markers (phosphorylated-Akt and phosphorylated-Erk) and increase in cleavage of caspase-3 and PARP (9).

The actions of calcitriol are mediated by the vitamin D receptor (VDR), a member of the nuclear receptor superfamily (11). VDR expression is observed in several endothelial cell types, including TDEC (9, 12, 13). Treatment with calcitriol induces up-regulation of VDR protein expression, promotes receptor phosphorylation and increases receptor trafficking into the nucleus in TDEC (9). Ligand-bound VDR heterodimerizes with the retinoid X receptor and interacts with specific DNA sequences to regulate gene expression (9, 14).

The physiological consequences of calcitriol/VDR disruption have been investigated in animals and humans deficient in vitamin D as well as those with VDR mutations (15–18). Defects in VDR structure, which impair the function of the receptor, are shown to be the molecular basis for the human vitamin D-resistant rickets (19, 20). The study of mice with targeted ablation of VDR has provided substantial insights into the role of the receptor in various calcitriol effects (11, 21–23). In the VDR knock-out (KO) mice, VDR ablation appears to increase sensitivity to mammary gland tumorigenesis and chemical-induced skin carcinogenesis. Thus, supporting the role of vitamin D signaling in tumor development (6, 24). Whether VDR plays a major role in calcitriol-mediated anti-proliferative effects on TDEC or tumor angiogenesis is unclear. Since formation of blood vessels in the tumor requires participation from the host cells (25, 26), in this study, we compared TDEC isolated from tumors derived from a cell line established from the transgenic adenocarcinoma of the mouse prostate model (TRAMP-C2) in VDR wild type (WT) and KO mice. TRAMP cells express wild type VDR but the endothelial cells recruited into the tumors will be determined by the hosts' genetic background.

Materials and Methods

Chemicals and reagents

Calcitriol (Hoffmann-LaRoche, Nutley, NJ) was reconstituted in 100% ethanol and stored, protected from light, under a layer of nitrogen gas at −70°C. All handling of calcitriol was performed with indirect lighting. Immediately prior to use, calcitriol was diluted to the final concentrations in tissue culture medium. For most application, calcitriol was used at 10 nM, a concentration that consistently shows anti-proliferative effects in multiple assays in a variety of tumor cell types. Albumin-GdDTPA (courtesy of Robert Brasch) was obtained from Contrast Media Laboratory, Department of Radiology, University of California at San Francisco (San Francisco, CA). This agent has been extensively characterized and used for experimental studies (27).

Animal models

A breeding colony of VDR KO mice was established from mice generously provided by Dr. Marie Demay (Harvard Medical School, Boston, MA). The phenotype of these mice, generated by targeted ablation of the second zinc finger of the DNA-binding domain of the VDR, resembles the human vitamin D-dependent rickets type II (11). Mice were genotyped by PCR amplification of DNA isolated from tail cuts using primers targeting exon 3 (second zinc finger region) for WT mice and the neomycin gene (replaces exon 3) for KO mice. All VDR KO and WT mice were fed with a diet containing 2% calcium, 1.25% phosphorus and 20% lactose with 2.2 IU vitamin D3/g (TD96348, Teklad, Madison, WI). This diet has been shown to normalize serum mineral homeostasis, bone growth and body weight in VDR KO mice (28). TRAMP C2 (TRAMP) cells were maintained in RPMI 1640 with 10% FBS and

1% penicillin/streptomycin (29). 2×10^6 TRAMP-2 cells were inoculated subcutaneously in 0.1 ml HBSS:Matrigel (1:1) solution into age-matched VDR WT and KO male mice. Tumor growth was monitored over time and tumor size was measured using calipers. Tumor volumes were calculated by the following formula: volume = (length × width^2)/2. After 31 days, tumors were harvested and processed for endothelial cell isolation, immunohistochemical or molecular studies. All mice breeding and handling were approved by the Institutional Animal Care and Use Committee at Roswell Park Cancer Institute.

Isolation of TDEC

Isolation and identification of TDEC from TRAMP tumors implanted in VDR WT and KO mice were performed using procedures described previously (9, 30). TDEC were cultured on 1% gelatin-coated flasks (Corning Glass Inc.) in DMEM /10% v/v FBS /1% penicillin and streptomycin. For all experiments, endothelial cells used were at low passage (< 8).

Immunohistochemistry

Endothelial CD31 staining—tumors were excised and immediately placed in zinc fixative (BD Biosciences Pharmingen, San Diego, CA) overnight, transferred to 70% ethanol, dehydrated, and embedded in paraffin. Sections 5 μm thick were stained after conventional deparaffinization, endogenous peroxidase quenching with 3% H_2O_2, and pretreatment with 0.03% casein in PBS with 500 μl/l Tween for 30 minutes at room temperature to block non-specific binding. Slides were counterstained with Harris hematoxylin (Poly Scientific, Bayshore, NY). Mouse CD31 was detected with rat monoclonal antibody (IgG2a; BD Biosciences Pharmingen) at 1:50 dilution in PBS for 60 minutes at 37°C. This was followed by the addition of biotinylated rabbit anti-rat IgG (BD Biosciences Pharmingen) at 1:100 dilution for 30 minutes, streptavidin peroxidase (Zymed, San Francisco, CA) for 30 minutes, and diaminobenzidine for 5 minutes. An isotype-matched control (10 μg/ml rat IgG) was used on a duplicate slide in place of the primary antibody as a negative control.

CD31/α-smooth muscle actin (SMA) double staining—frozen sections (6 μm) were cut and stored at −80° C until assay was run. The slides were thawed quickly and fixed for 10 minutes in cold acetone (−20°C). After blocking, α-SMA antibody was used at 1/250 for 30 minutes and was detected by biotinylated goat anti-rabbit secondary antibody 25 minutes followed by streptavidin peroxidase for additional 25 minutes. 3,3'-diaminobenzidine (DAB) was used as the chromogen for α-SMA. After a second blocking step, sections were incubated with CD31 (BD Biosciences Pharmingen) at 5μg/ml for 30 minutes followed by biotinylated anti-rat secondary antibody for 25 minutes and alkaline phosphatase-conjugated streptavidin reagent for 25 minutes. The chromogen Fast Red was used to detect CD31. An isotype-matched control (2 μg/ml rabbit IgG and 5 μg/ml rat IgG) was used on a duplicate slide in place of the primary antibody as a negative control.

Vessel morphological analysis

Mean vessel density—Intratumoral blood vessels were counted on cross sections of tumors stained with endothelial cell marker CD31.Using light microscope, images of 5 fields at consistent locations for each sample were taken at magnification ×100. The average number of microvessels per field was calculated using Image J software (National Institute Health, Bethesda, MD). Vessels with a clearly defined lumen or a well-defined linear vessel shape were counted. Single endothelial cells were not counted as vessels.

Vessel lumen area—Images of vessels at the locations described above were taken at high-power field (magnification, ×400). Vessel lumen area was determined using the

software Analyze 7.0 (AnalyzeDirect, Overland Park, KS), by measuring the vessel lumen circumference stained with CD31 antibody.

Pericyte coverage analysis—Images of vessels in sections stained with CD31 and α-SMA were taken at high-power field (magnification, ×400). CD31- and α-SMA-positive areas were measured for each vessel using software Analyze 7.0. Pericyte coverage for each vessel was calculated using the formula: (CD31 and α-SMA overlapping area)/ (total CD31 positive area).

Contrast-enhanced magnetic resonance imaging

Magnetic resonance imaging (MRI) of tumor-bearing mice was carried out in a 4.7T horizontal bore scanner (General Electric NMR Instruments, Fremont, CA). We have previously described the imaging protocol for calculating tumor vascular volume using the intravascular contrast agent, albumin-GbDTPA (27). Regional precontrast T1-values were calculated from a series of three preliminary images acquired prior to contrast agent administration. Following these baseline acquisitions, albumin-GdDTPA (0.1 mmol/kg) was injected *via* tail-vein and a second series of five postcontrast images was acquired for ~45 minutes, as described previously (27). Image processing and analysis were carried out using commercially available software (Analyze PC, Version 7.0, AnalyzeDirect, Lenexa, KS). Regions of interest (ROI) of tumors, kidneys, and muscle tissues were manually drawn on the images and object maps of the ROI constructed. The longitudinal relaxation rate (R1 = 1/T1) for each ROI was computed using MATLAB (Version 7.0; Math Works, Inc., Natick, MA), and source codes were developed by RPCI Preclinical Imaging Resource. Linear regression analysis of the change in RI (ΔRI) over the 45 minute period was used to compare vascular volume and permeability (27) and differences between tumors in WT (n=7) and KO mice (n=8) analyzed for statistical significance using Prism (Version 5.00, GraphPad Prism, San Diego, CA).

In vivo Evans blue dye assay

Mice received intracardiac injections of 200 μl of Evans blue dye (0.5%) (Sigma, St. Louis, MO) for five minutes while under anesthesia. After sacrifice, tumors and livers were collected and incubated with formamide (Fisher, Pittsburgh, PA) at 55 °C overnight. The amount of dye extracted from each samples was quantitated by spectrophotometry (Spectra Max 340PC) at 610 nm. Data were normalized with sample weight and data obtained from liver.

FITC-dextran permeability assay

Mice were given intracardiac injection with 200 μl of saline containing 2 μM lysine-fixable FITC-labeled dextran (FITC-D 2×10^6 MW, Molecular Probes, Eugene, OR) for 5 minutes followed by 2 minutes of 0.05 M citrate in 1% paraformaldehyde (pH 3.5) while under anesthesia. After sacrifice, tumors and livers were collected immediately and frozen using O.C.T. compound. 5 μm thick sections were prepared and mounted in VectaShield with DAPI (Vector Laboratories, Burlingame, CA) followed by analysis with a confocal microscopy (Leica TCS SP2, Leica Microsytems, Bannockburn, IL).

Tetrazolium salt 3-(4,5-dimethylthiazol-2-yl)-2,5-diphenyl tetrazolium bromide (MTT) assay

TDEC were plated at the range of $1–2 \times 10^3$ cells/well into 96-well tissue culture plates (Corning Glass, Lowell, MA) and incubated at 37°C in a humidified atmosphere containing 5% CO_2. After 24 hours post plating, cells were either treated for 48 hours with vehicle or varying doses of calcitriol. Cells were harvested by adding 20 μl of 0.5% MTT (Sigma) for 3 hours at 37°C. The medium was removed, and the cells were solubilized with 10% SDS/10

mM HCl for overnight at 37°C. The absorbance was read with an ELISA reader (Spectra Max 340PC) at 490 nm.

Western blot analysis

24 hours post plating, the cells were treated with vehicle or 10 nM calcitriol. After 48 hours, the cells were harvested and whole cell lysates were prepared using lysis buffer as described previously (9). For *in vivo* tumor and Matrigel plug specimens, protein lysates were prepared using CelLytic Lysis Buffer (Sigma). Protein samples (30 μg) were resolved by SDS-PAGE, and transferred overnight to polyvinylidene difluoride membranes. Western blot analysis was performed as previously described. Antibodies used include VDR (Santa Cruz, CA), HIF-1alpha (ABR, Golden, CO), VEGF (Santa Cruz), VEGFR2 (Cell Signaling, Denvers, MA), Ang1 (US Biological, Swampscott, MA), Tie1 (Santa Cruz), Tie2 (Santa Cruz), PDGF-B (Santa Cruz), PDGFR beta (Santa Cruz). Anti-rabbit and anti-mouse horseradish peroxidase-conjugated secondary antibodies were purchased from Amersham Life Sciences (Piscataway, NJ) and actin was detected using the actin kit from Oncogene Research Products (Cambridge, MA).

Enzyme-Linked ImmunoSorbent Assay (ELISA)

Protein lysates were prepared from tumors using CelLytic Lysis Buffer (Sigma). All ELISA procedures were performed using ELISA development kits, murine VEGF (PeproTech Inc., Rocky Hill, NJ), murine HIF1 alpha (R&D Systems, Minneapolis, MN), murine Ang1 (R&D Systems) and murine PDGF-B (R&D Systems) following the manufacture's instruction. Data were collected from at least 5 samples from each group were measured in triplicates.

24-hydroxylase promoter-luciferase reporter assay

Cells were plated on 48 wells plate and cultured for 24 hours in 5% charcoal-stripped media and then treated for 3 hours with a constant dose of adenovirus containing beta-galactosidase and adenovirus containing 24-hydroxylase promoter-luciferase construct or adenoviral empty vector control in serum-free media. The cells were treated with varying doses of calcitriol for 48 hours in 5% charcoal-stripped media. Cells were harvested and cell lysates were obtained as described previously (9). The cell lysates were then subjected to Luciferase Assay Reagent (Promega, Madison, WI) and the light produced were measured with a luminometer (Veritas™ Microplate Luminometer, Sunnyvale, CA). Beta-galactosidase activity was obtained using Beta-Galactosidase Enzyme Assay System (Promega) and the absorbance was measured with an ELISA reader (Spectra Max 340PC) at 520 nm. The relative luciferase unit (RLU) was obtained by normalizing the luciferase unit with the activity of beta-galactosidase and total protein from each lysate.

Cell cycle analysis

Endothelial cells were plated and treated at a final concentration 10 nM calcitriol. Cells were harvested 48 hours after treatment by trypsinization, washed using PBS and fixed with 70% ethanol. The cells were RNase-treated prior to staining with 400 μl of 50 mg/ml propidium iodide (PI) (Sigma) in PBS solution, filtered through 30 μm nylon mesh, and analyzed by flow cytometry using a BD FACScan. Cell cycle analysis was performed using ModFit™ software.

Statistical analysis

Differences between groups were analyzed for statistical significance using the Student t's test (two-tailed). All data were expressed as the mean (with standard deviation) of at least 3 determinants, unless stated otherwise.

Results

TDEC isolated from VDR KO mice are not sensitive to calcitriol-mediated growth inhibition

We demonstrated that calcitriol exerts growth inhibitory effects on TDEC by inducing G_0-G_1 cell cycle arrest and apoptosis (9). To determine the role of VDR on these effects, we isolated TDEC from TRAMP-2 tumors grown for 30 days in WT and KO mice, using methods previously described (29). As shown in Fig. 1*A*, there was no obvious difference in cell morphology of TDEC when isolated from different VDR genotype mice. The doubling time for each cell type was similar (data not shown). Upon treatment with calcitriol, VDR expression was induced in TDEC isolated from WT but not in those from KO mice (Fig. 1*B*). Using the 24-hydroxylase promoter-luciferase reporter, we demonstrated that in TDEC expressing VDR, but not those from KO mice, calcitriol transactivated CYP24, a calcitriol responsive gene (Fig.1*C*). These results indicate that endothelial cells derived from TRAMP tumors grown in VDR KO mice were VDR negative and could not activate VDR-mediated signaling pathway.

TDEC from these mice were treated with 0–500 nM of calcitriol for 48 hours and cell viability was determined using the MTT assay. TDEC expressing VDR growth inhibited in a dose-dependent manner (Fig. 1*D*). However, in the absence of VDR, TDEC were minimally affected by similar treatment (Fig. 1*D*). The growth inhibition observed in TDEC expressing VDR was accompanied by an induction of G_0-G_1 cell cycle arrest, as measured by propidium iodide staining (Table 1). An increase of G_0-G_1 phase cells from 45% to 77% and a decrease of S phase cells from 53% to 23% were observed in calcitriol-treated TDEC from WT mice (Table 1). These effects were not observed in TDEC from KO mice. These results indicate that calcitriol-mediated growth inhibition in TDEC is a VDR-dependent event.

Vessels in TRAMP-2 tumors in VDR KO mice are enlarged and have lower pericyte coverage

Detailed examination of the tumor vascular morphology was performed by immunohistochemical staining of tumor sections for the endothelial cell marker, CD31. While mean vessel density was not different between the two groups, vessel lumen size and percentage vessel area per field were higher in tumors of KO mice, when compared to WT mice ($P < 0.001$) (Table 2). Using CD31 and alpha-SMA (pericyte marker) double staining to measure pericyte coverage vessels in tumor of VDR KO mice have less pericyte coverage when compared to those in WT mice (Fig 2B). In WT mice, the average pericyte coverage of the vessels is 39% while tumor vessels in KO mice have approximately 11% pericyte coverage (Table 2). These findings suggest a lesser degree of vessel maturation in VDR KO vessels. In addition to the microvessels, there were also a proportion of enlarged vessels found in KO mice and these are not obvious in WT animals (Fig. 2*A*, Table 2).

Tumors in VDR WT and KO mice have different vascular properties and size

To evaluate the functional implications of these morphologic differences, we examined tumor perfusion using contrast-enhanced MR imaging. Change in longitudinal relaxation rates (ΔR_1) of tumors implanted in WT and KO mice were plotted as a function of time and parameters of vascular volume (Y-intercept) and permeability (slope) calculated. The vascular volume of TRAMP-C2 tumors implanted in KO mice (0.1953±0.005) was significantly higher than tumors implanted in WT (0.1047±0.0205) ($P<0.0001$) (Fig. 3A). There was not a difference in vascular permeability between the two types of tumors (Figure 3*A*). No significant change in the longitudinal relaxation rates was observed in kidneys and muscle tissues between VDR WT and VDR KO mice (data not shown).

We further evaluated vascular volume and permeability using quantitative *in vivo* Evans blue dye assay and qualitative FITC-dextran staining. Tumors from VDR KO mice showed a significant higher Evans blue dye content (P=0.029), indicating a higher vascular volume in these tumors (Fig 3B). Confocal microscopy analysis of FITC-dextran stained tumor vasculature showed a higher degree of plasma extravasation in KO vs. WT animals (Fig. 3*C*). FITC-dextran stained vasculature in the liver served as a control for injection of the dyes.

We compared the growth of TRAMP-C2 tumors in VDR WT and KO mice. Tumors were palpable around day 14-post inoculation; subsequently, tumor measurement was performed twice a week (Fig. 3*D*). From day 18 to day 31, TRAMP-C2 tumors in KO mice were larger than those in WT animals (P = 0.018).

Abnormal tumor vasculature in VDR KO mice is associated with increased HIF-1 alpha, VEGF, Ang 1 and PDGF-B expression

Angiogenesis is a process governed by complex signaling pathways that promote endothelial cell proliferation and vascular maturation (25). To determine if the observed differences in angiogenesis between WT and KO tumors were related to dysregulation of angiogenic signaling pathways, we examined hypoxia-induced factor-1 (HIF-1) alpha, vascular endothelial growth factor (VEGF), angiopoeitin 1 (Ang1) and platelet-derived growth factor (PDGF)-B protein expression from the tumor lysates. Tumors from VDR KO mice exhibited a significantly higher level of HIF-1 alpha protein when compared to WT mice (P = 0.01) as measured by ELISA (Fig. 4*A*). There was a significant increase in VEGF expression in tumors from KO mice when compared to WT (Fig. 4*B* and *E*). No significant change was observed in VEGFR2 protein level between the two groups (Fig. 4*E*). Higher expression of Ang1 (Fig. 4*C*, *E*) and PDGF-BB (the dimer form) was also observed (Fig. 4*D*, *E*) in tumors from VDR KO mice as compared to the WT counterpart. No differences were observed in the expression of the receptors for Ang1 (Tie1 and Tie2) and PDGF-BB (PDGF-R beta) between these tumors (Fig. 4*E*). Increased expression of these pro angiogenic signaling molecules could at least in part account for the observed tumor vasculature characteristics in VDR KO mice.

Discussion

Calcitriol exerts profound anti-proliferative effects on TDEC by inducing G_0-G_1 cell cycle arrest and apoptosis (8, 9). In TDEC, treatment with calcitriol up-regulates VDR protein expression and activates VDR signaling pathway (9). This study in VDR KO mice demonstrates that VDR plays a major role in calcitriol-mediated anti-proliferative effects in TDEC and in the development of tumor angiogenesis *in vivo*. TDEC isolated from tumors implanted in VDR WT, but not those from KO mice, show/demonstrate enhanced VDR protein expression and are growth inhibited by calcitriol. Calcitriol treatment induced G_0-G_1 cell cycle arrest in TDEC expressing VDR but not VDR KO TDEC. In calcitriol-treated TDEC from VDR KO mice, the lack of luciferase signal from the promoter reporter assay suggests that calcitriol-activated VDR may be involved in regulating the transcription of various target genes governing cell growth (31).

Absence of VDR in tumor-infiltrating vessels results in a more aberrant vasculature. Compared to WT animals, the tumor vessels in the KO mice are enlarged, are associated with fewer pericytes and these tumors contain increased content of angiogenic factors such as HIF-1 alpha, VEGF, Ang1 and PDGF-BB.

During rapid growth, tumor cells encounter hypoxic conditions which result in the induction of HIF-1 alpha (32). HIF-1 alpha can act as a transcriptional activator for various genes

including VEGF (33). VEGF is a potent endothelial cell growth factor and survival molecule (34). Studies using transgenic VEGF mice and adenoviral-mediated ectopic VEGF over-expression animal model revealed that excessive amount of VEGF can result in enlarged and highly permeable vascular beds (35,36). Similarly, in mice over-expressing Ang1, vessels were also dramatically enlarged compared to the control mice (37,38). Although Ang1 does not stimulate proliferation of endothelial cells (39), Ang1 can induce endothelial migration, tube formation, sprouting and survival following various apoptotic insults (40). Ang1 synergized with VEGF to activate PI3K and Akt signaling to promote endothelial cell survival (41). Consistent with these studies, our observation of significantly enlarged tumor vessels in VDR KO mice may be attributed to the high level of VEGF and Ang1 within the tumor microenvironment.

Despite high expression of VEGF observed in tumors of VDR KO mice, our studies did not reveal a significant increase in vascular permeability in these tumors. These findings could be explained by the Ang1 over-expression in these tumors since studies by others have shown that vessels stimulated by Ang1 are resistant to plasma leakage (38). When both VEGF and Ang1 were over-expressed at the same time, the anti-leakage of Ang1 phenotype appears to dominate (38, 42). Taken together, we conclude that complete loss of VDR signaling results in aberrant angiogenic signaling pathways in the tumor microenvironment.

We demonstrated that tumor vessels in KO animals were covered with less pericytes when compared to those in WT animals. Pericytes regulate endothelial cell proliferation, survival, migration and differentiation, and also modulate blood flow and vascular permeability. It has been demonstrated that lack of pericyte coverage may represent a window of plasticity for further vessel remodeling (43). Therefore, the vessels in VDR KO mice may be more responsive to mitogenic and survival signals. However, the lower pericyte coverage observed in VDR KO mice is contrary to the increase of pericyte recruiting factor, PDGF-BB expression in these tumors. It has been shown that endothelial cells secrete PDGF-BB which promotes pericyte recruitment in a paracrine fashion (43). Interestingly, ectopic PDGF-BB expression could disrupt endothelial-pericyte interactions and may lead to abnormalities in pericyte attachment and in vessel remodeling (43). In addition to promoting pericyte recruitment, PDGF-BB induces intratumoral lymphangiogenesis and lymphatic metastasis in the murine fibrosarcoma model (44), promotes angiogenesis and glial tumorigenesis (45), and directly promotes the growth of prostate cancer cells (46). *In vitro* and *in vivo* studies show that targeting this signaling pathway, using PDGF receptor tyrosine kinase inhibitors (such as STI571), can enhance paclitaxel-mediated regression of prostate tumors (47). Therefore, the enhanced PDGF-BB expression within the TRAMP-C2 tumors in VDR KO mice may not only affect pericyte recruitment but also may lead to increased neovascularization and tumor cell growth.

The role of VDR signaling in regulating these angiogenic pathways is not well characterized. In various human cancer cells, calcitriol inhibits HIF-1 alpha protein expression and HIF-1 alpha target genes such as VEGF, endothelin-1 and glucose transporter-1 (48). Further, there are DR3 type vitamin D response element-like sequence in the promoter region of the rat VEGF gene (48); therefore, it is possible that calcitriol modulates VEGF expression at the transcriptional level (49–50). Whether Ang1 and PDGF-B expression are also regulated through direct VDR-DNA interaction remains to be elucidated. In calcitriol-treated TDEC WT cells, we observed a reduction of VEGF, Ang1 and PDGF-BB expression but this is not seen in TDEC KO cells. This model of TDEC isolated from different tumor microenvironments will allow for a direct examination of the role of VDR in mediating calcitriol effects on angiogenic signaling pathways.

Our studies also contribute to the increasing evidence indicating that host cells contribute to tumor growth. In addition to the endothelial cells, there are other host cells present in the tumor microenvironment, e.g. pericytes, stromal cells and immune cells. The role of VDR signaling in the interactions among these cell types and tumor cells in tumorigenesis remains to be elucidated. In this model, we compared vasculature from the same tumor cells grown in different VDR genetic background. The differences of phenotype observed could be directly attributed to the VDR activity in the host cells. Our studies provide *in vivo* molecular evidence that calcitriol-VDR signaling has substantial impact on tumor angiogenesis and is required for the growth inhibitory effects on TDEC.

Acknowledgments

Grant support: NIH/NCI CA67267, CA85142 and CA95045 and DOD grant PCRP050202.

We thank Harold Dvorak, Mohamed Khan, Shaozeng Zhang and Arup Bhattacharya for discussion and Marie Demay for providing VDR KO mice colony. We are also grateful to Sandra Buitrago and the rest of RPCI Department of Laboratory Animal Resource for assistance in animal husbandry; and Mary Vaughan and Histology Laboratory Services staff for immunohistochemical support.

References

1. van den Bemd GJ, Pols HA, van Leeuwen JP. Anti-tumor effects of 1,25-dihydroxyvitamin D3 and vitamin D analogs. Curr Pharm Des. 2000; 6:717–732. [PubMed: 10828303]
2. Johnson CS, Muindi JR, Hershberger PA, Trump DL. The antitumor efficacy of calcitriol: preclinical studies. Anticancer Res. 2006; 26:2543–2549. [PubMed: 16886662]
3. Koeffler HP, Hirji K, Itri L. 1,25-Dihydroxyvitamin D3: in vivo and in vitro effects on human preleukemic and leukemic cells. Cancer Treat Rep. 1985; 69:1399–1407. [PubMed: 2416438]
4. Hershberger PA, Modzelewski RA, Shurin ZR, Rueger RM, Trump DL, Johnson CS. 1,25-Dihydroxycholecalciferol (1,25-D3) inhibits the growth of squamous cell carcinoma and down-modulates p21(Waf1/Cip1) in vitro and in vivo. Cancer Res. 1999; 59:2644–2649. [PubMed: 10363987]
5. Lokeshwar BL, Schwartz GG, Selzer MG, et al. Inhibition of prostate cancer metastasis in vivo: a comparison of 1,23-dihydroxyvitamin D (calcitriol) and EB1089. Cancer Epidemiol Biomarkers Prev. 1999; 8:241–248. [PubMed: 10090302]
6. Welsh J. Vitamin D and breast cancer: insights from animal models. Am J Clin Nutr. 2004; 80:1721S–1724S. [PubMed: 15585794]
7. Diaz GD, Paraskeva C, Thomas MG, Binderup L, Hague A. Apoptosis is induced by the active metabolite of vitamin D3 and its analogue EB1089 in colorectal adenoma and carcinoma cells: possible implications for prevention and therapy. Cancer Res. 2000; 60:2304–2312. [PubMed: 10786699]
8. Bernardi RJ, Johnson CS, Modzelewski RA, Trump DL. Antiproliferative effects of 1alpha,25-dihydroxyvitamin D(3) and vitamin D analogs on tumor-derived endothelial cells. Endocrinology. 2002; 143:2508–2514. [PubMed: 12072382]
9. Chung I, Wong MK, Flynn G, Yu WD, Johnson CS, Trump DL. Differential antiproliferative effects of calcitriol on tumor-derived and matrigel-derived endothelial cells. Cancer Res. 2006; 66:8565–8573. [PubMed: 16951169]
10. Flynn G, Chung I, Yu WD, et al. Calcitriol (1,25-Dihydroxycholecalciferol) selectively inhibits proliferation of freshly isolated tumor-derived endothelial cells and induces apoptosis. Oncology. 2007; 70:447–457. [PubMed: 17237620]
11. Li YC, Pirro AE, Amling M, et al. Targeted ablation of the vitamin D receptor: an animal model of vitamin D-dependent rickets type II with alopecia. Proc Natl Acad Sci U S A. 1997; 94:9831–9835. [PubMed: 9275211]
12. Merke J, Milde P, Lewicka S, et al. Identification and regulation of 1,25-dihydroxyvitamin D3 receptor activity and biosynthesis of 1,25-dihydroxyvitamin D3. Studies in cultured bovine aortic

endothelial cells and human dermal capillaries. J Clin Invest. 1989; 83:1903–1915. [PubMed: 2542376]

13. Chung I, Karpf AR, Muindi JR, et al. Epigenetic silencing of CYP24 in tumor-derived endothelial cells contributes to selective growth inhibition by calcitriol. J Biol Chem. 2007; 282:8704–8714. [PubMed: 17244627]
14. Christakos S, Raval-Pandya M, Wernyj RP, Yang W. Genomic mechanisms involved in the pleiotropic actions of 1,25-dihydroxyvitamin D3. Biochem J. 1996; 316:361–371. [PubMed: 8687373]
15. Dostal LA, Toverud SU. Effect of vitamin D3 on duodenal calcium absorption in vivo during early development. Am J Physiol. 1984; 246:G528–G534. [PubMed: 6547027]
16. Halloran BP, DeLuca HF. Effect of vitamin D deficiency on fertility and reproductive capacity in the female rat. J Nutr. 1980; 110:1573–1580. [PubMed: 7400847]
17. Mathews CH, Brommage R, DeLuca HF. Role of vitamin D in neonatal skeletal development in rats. Am J Physiol. 1986; 250:E725–E730. [PubMed: 3717332]
18. Balsan S, Garabedian M, Larchet M, et al. Long-term nocturnal calcium infusions can cure rickets and promote normal mineralization in hereditary resistance to 1,25-dihydroxyvitamin D. J Clin Invest. 1986; 77:1661–1667. [PubMed: 3009551]
19. Beer S, Tieder M, Kohelet D, et al. Vitamin D resistant rickets with alopecia: a form of end organ resistance to 1,25 dihydroxy vitamin D. Clin Endocrinol (Oxf). 1981; 14:395–402. [PubMed: 6266702]
20. Malloy, PJ.; Pike, JW.; Feldman, D. Hereditary 1,25-dihydroxyvitamin D resistant rickets. In: Feldman, D.; Pike, JW.; Glorieux, FH., editors. Vitamin D. New York: Elsevier Academic Press; 2005. p. 1207-1238.
21. Yoshizawa T, Handa Y, Uematsu Y, et al. Mice lacking the vitamin D receptor exhibit impaired bone formation, uterine hypoplasia and growth retardation after weaning. Nat Genet. 1997; 16:391–396. [PubMed: 9241280]
22. Van Cromphaut SJ, Dewerchin M, Hoenderop JG, et al. Duodenal calcium absorption in vitamin D receptor-knockout mice: functional and molecular aspects. Proc Natl Acad Sci U S A. 2001; 98:13324–13329. [PubMed: 11687634]
23. Erben RG, Soegiarto DW, Weber K, et al. Deletion of deoxyribonucleic acid binding domain of the vitamin D receptor abrogates genomic and nongenomic functions of vitamin D. Mol Endocrinol. 2002; 16:1524–1537. [PubMed: 12089348]
24. Zinser GM, Sundberg JP, Welsh J. Vitamin D(3) receptor ablation sensitizes skin to chemically induced tumorigenesis. Carcinogenesis. 2002; 23:2103–2109. [PubMed: 12507934]
25. Folkman J. Tumor angiogenesis: therapeutic implications. N Engl J Med. 1971; 285:1182–1186. [PubMed: 4938153]
26. Rafii S, Avecilla S, Shmelkov S, et al. Angiogenic factors reconstitute hematopoiesis by recruiting stem cells from bone marrow microenvironment. Ann N Y Acad Sci. 2003; 996:49–60. [PubMed: 12799282]
27. Seshadri M, Mazurchuk R, Spernyak JA, Bhattacharya A, Rustum YM, Bellnier DA. Activity of the vascular-disrupting agent 5,6-dimethylxanthenone-4-acetic acid against human head and neck carcinoma xenografts. Neoplasia. 2006; 8:534–542. [PubMed: 16867215]
28. Li YC, Amling M, Pirro AE, et al. Normalization of mineral ion homeostasis by dietary means prevents hyperparathyroidism, rickets, and osteomalacia, but not alopecia in vitamin D receptor-ablated mice. Endocrinology. 1998; 139:4391–4396. [PubMed: 9751523]
29. Foster BA, Gingrich JR, Kwon ED, Madias C, Greenberg NM. Characterization of prostatic epithelial cell lines derived from transgenic adenocarcinoma of the mouse prostate (TRAMP) model. Cancer Research. 1997; 57:3325–3330. [PubMed: 9269988]
30. Modzelewski RA, Davies P, Watkins SC, Auerbach R, Chang MJ, Johnson CS. Isolation and identification of fresh tumor-derived endothelial cells from a murine RIF-1 fibrosarcoma. Cancer Res. 1994; 54:336–339. [PubMed: 8275463]
31. White JH. Profiling 1,25-dihydroxyvitamin D3-regulated gene expression by microarray analysis. J Steroid Biochem Mol Biol. 2004; 89–90:239–244.

32. Gordan JD, Simon MC. Hypoxia-inducible factors: central regulators of the tumor phenotype. Curr Opin Genet Dev. 2007; 17:71–77. [PubMed: 17208433]
33. Mabjeesh NJ, Amir S. Hypoxia-inducible factor (HIF) in human tumorigenesis. Histol Histopathol. 2007; 22:559–572. [PubMed: 17330811]
34. Ferrara N. VEGF and the quest for tumour angiogenesis factors. Nat Rev Cancer. 2002; 2:795–803. [PubMed: 12360282]
35. Nagy JA, Feng D, Vasile E, et al. Permeability properties of tumor surrogate blood vessels induced by VEGF-A. Lab Invest. 2006; 86:767–780. [PubMed: 16732297]
36. Thurston G, Suri C, Smith K, et al. Leakage-resistant blood vessels in mice transgenically overexpressing angiopoietin-1. Science. 1999; 286:2511–2514. [PubMed: 10617467]
37. Thurston G, Wang Q, Baffert F, et al. Angiopoietin 1 causes vessel enlargement, without angiogenic sprouting, during a critical developmental period. Development. 2005; 132:3317–3326. [PubMed: 15958513]
38. Suri C, McClain J, Thurston G, et al. Increased vascularization in mice overexpressing angiopoietin-1. Science. 1998; 282:468–471. [PubMed: 9774272]
39. Davis S, Aldrich TH, Jones PF, et al. Isolation of angiopoietin-1, a ligand for the TIE2 receptor, by secretion-trap expression cloning. Cell. 1996; 87:1161–1169. [PubMed: 8980223]
40. Metheny-Barlow LJ, Li LY. The enigmatic role of angiopoietin-1 in tumor angiogenesis. Cell Res. 2003; 13:309–317. [PubMed: 14672554]
41. Benjamin LE. The controls of microvascular survival. Cancer Metastasis Rev. 2000; 19:75–81. [PubMed: 11191067]
42. Thurston G. Complementary actions of VEGF and angiopoietins on blood vessel permeability and growth in mice. J Anat. 2002; 200:529. [PubMed: 17103730]
43. Benjamin LE, Hemo I, Keshet E. A plasticity window for blood vessel remodelling is defined by pericyte coverage of the preformed endothelial network and is regulated by PDGF-B and VEGF. Development. 1998; 125:1591–1598. [PubMed: 9521897]
44. Cao R, Bjorndahl MA, Religa P, et al. PDGF-BB induces intratumoral lymphangiogenesis and promotes lymphatic metastasis. Cancer Cell. 2004; 6:333–345. [PubMed: 15488757]
45. Shih AH, Holland EC. Platelet-derived growth factor (PDGF) and glial tumorigenesis. Cancer Lett. 2006; 232:139–147. [PubMed: 16139423]
46. Nazarova N, Golovko O, Blauer M, Tuohimaa P. Calcitriol inhibits growth response to Platelet-Derived Growth Factor-BB in human prostate cells. J Steroid Biochem Mol Biol. 2005; 94:189–196. [PubMed: 15862965]
47. Uehara H, Kim SJ, Karashima T, et al. Effects of blocking platelet-derived growth factor-receptor signaling in a mouse model of experimental prostate cancer bone metastases. J Natl Cancer Inst. 2003; 95:458–470. [PubMed: 12644539]
48. Ben-Shoshan M, Amir S, Dang DT, Dang LH, Weisman Y, Mabjeesh NJ. 1 alpha,25-dihydroxyvitamin D3 (Calcitriol) inhibits hypoxia-inducible factor-1/vascular endothelial growth factor pathway in human cancer cells. Mol Cancer Ther. 2007; 6:1433–1439. [PubMed: 17431122]
49. Haussler MR, Whitfield GK, Haussler CA, et al. The nuclear vitamin D receptor: biological and molecular regulatory properties revealed. J Bone Miner Res. 1998; 13:325–349. [PubMed: 9525333]
50. Mantell DJ, Owens PE, Bundred NJ, Mawer EB, Canfield AE. 1 alpha,25-dihydroxyvitamin D(3) inhibits angiogenesis in vitro and in vivo. Circ Res. 2000; 87:214–220. [PubMed: 10926872]

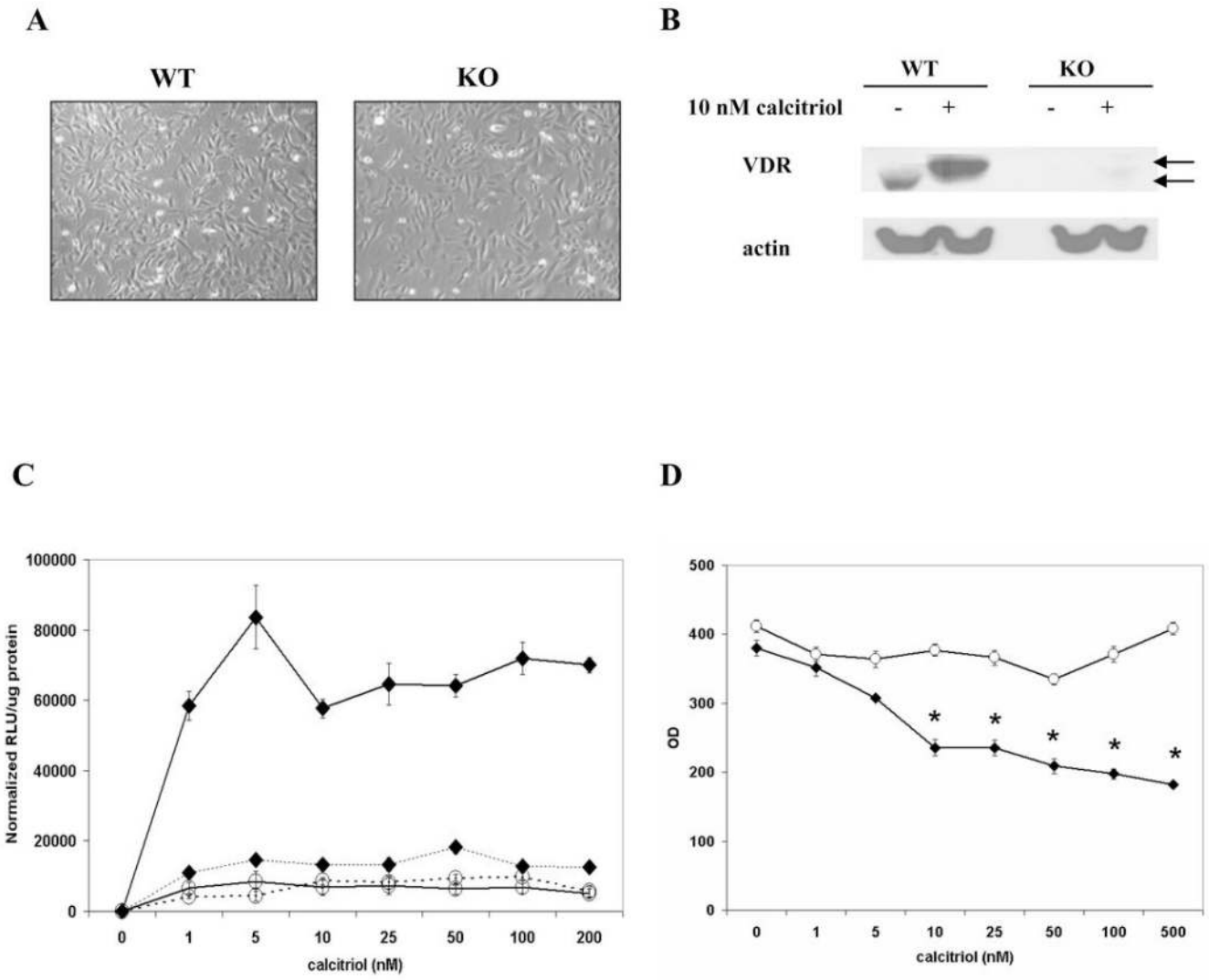

Fig. 1. TDEC expressing VDR is more sensitive to growth inhibitory effects by calcitriol

A, Phase contrast pictures showing no significant obvious difference in cell morphology of TDEC isolated from VDR WT or KO mice. *B*, VDR protein expression (arrows) was observed in 48 hr calcitriol-treated TDEC isolated from VDR WT but not KO mice as shown by Western blot analysis. *C*, Transactivation activity of VDR is observed in TDEC expressing VDR (◆) but not in those from KO mice (○). TDEC were transfected with a constant dose of adenoviral 24-hydroxylase promoter luciferase reporter and adenoviral β-galactosidase expression vector for 3 hrs before treatment with vehicle (dotted lines) or 10 nM calcitriol (solid lines) for 48 hr. Luminescence data were normalized with β-galactosidase activities, and the empty adenoviral control vector showed minimal luciferase activity (data not shown). *D*, The effects of 48 hr treatment of 1–500 nM calcitriol on cell viability as measured by MTT assay. TDEC isolated from VDR WT (◆) but not those from KO mice (○) were responsive to the anti-proliferative effects of calcitriol. *, $P < 0.001$ (Student's t test). *RLU*, relative luciferase unit. Representative of three independent experiments.

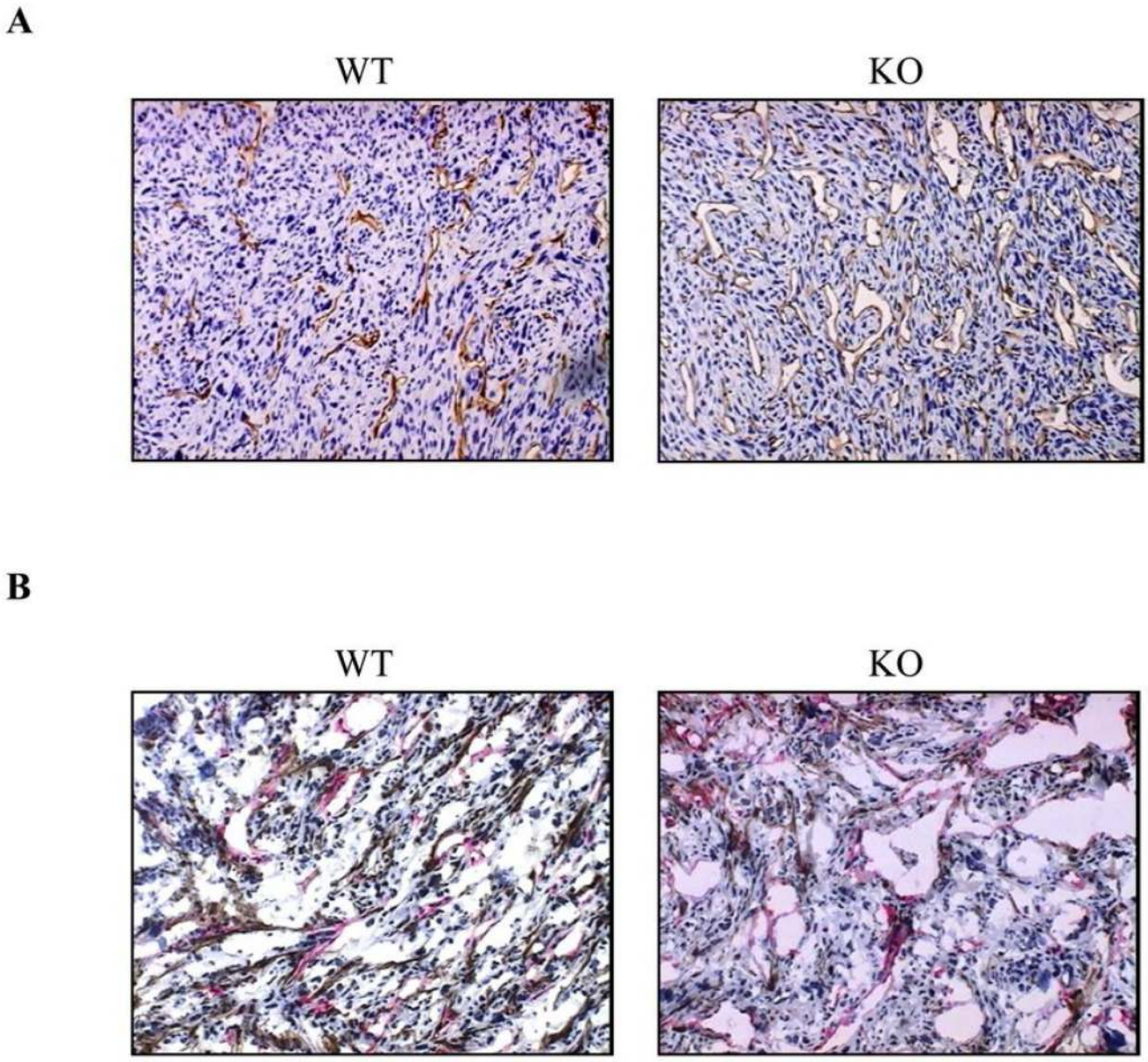

Fig. 2. Enlargement of tumor vessels in TRAMP tumors in VDR KO mice is associated with lower pericyte coverage

A, Representative of endothelial marker CD31-stained vessels (brown) found in tumors implanted in VDR WT and KO mice were shown. Magnification, ×100. *B*, Representative of endothelial marker CD31 (pink) and pericyte marker α-smooth muscle actin (brown) positive vessels found in tumors in both VDR WT and KO mice. Magnification, ×100.

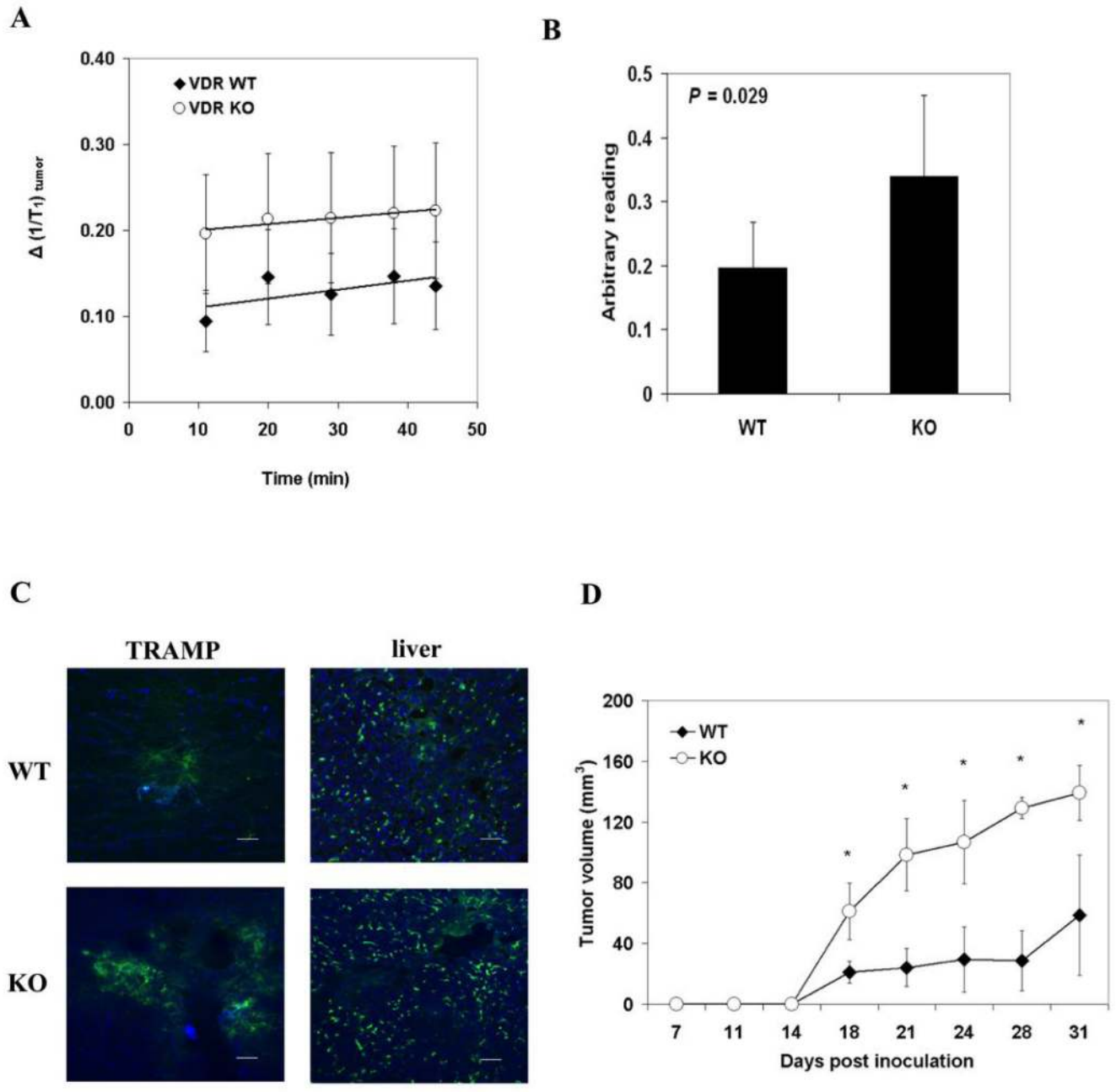

Fig. 3. Difference in blood volume, vascular leakiness and tumor size of tumors in VDR WT and KO mice

A, Change in T1 relaxation rates (ΔR_1) over time of TRAMP tumors in VDR WT (◆) and KO (○) mice. Vascular volume and permeability values were calculated from ΔR_1 using linear regression analysis. Analysis of the slopes showed a slight, but not significant difference in permeability between the two groups. Significant differences were seen between the vascular volumes (Y-intercept) of tumors in VDR WT and KO mice ($P < 0.001$). *B*, Modified *in vivo* Evans blue dye assay showed a significant increase in Evans blue dye content in tumors from VDR KO compared to WT. Animals were given 0.2 ml 0.5% Evans blue intracardiacally under anesthesia for 5 min before sacrificied. The dye

from tumors was extracted using formamide and readings were normalized with those from the livers. Data shown were from at least 3–5 animals per group. *C*, Confocal microscopy analysis shows a more extensive leakage of FITC-dextran from tumor vasculature in VDR KO than in WT animals. Animals were given 0.2 ml 2 μM FITC-dextran in saline intracardically before fixation with paraformaldehyde. Livers were used as a control for sufficient systemic delivery of the dye. Data shown were representative of three independent experiments. Scale bar, 200 μm. *D*, Tumors in VDR KO mice is larger than those in WT mice. 2×10^6 of TRAMP cells were implanted subcutaneously into VDR WT (◆) and KO (○) mice. The growth of the tumors, as measured by the tumor size, was monitored over time. There were at least 4–6 animals per group, and the data shown is representative of two independent experiments.

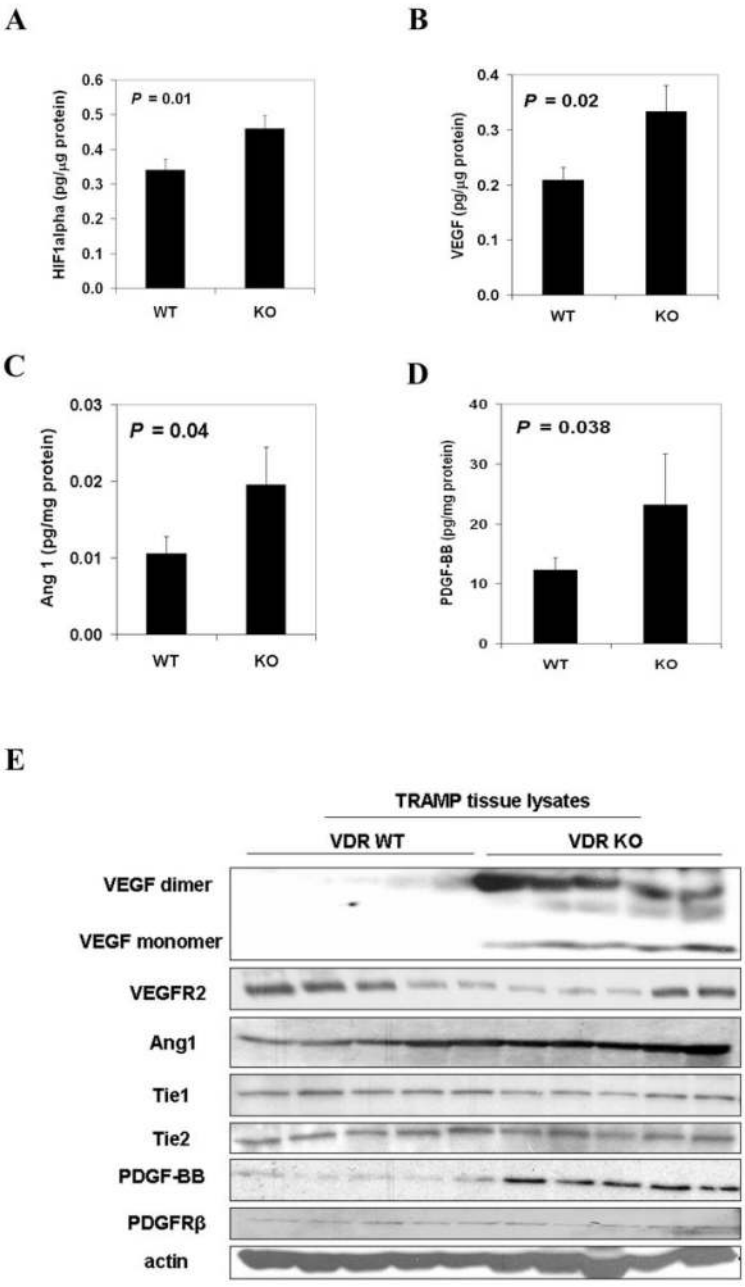

Fig. 4. Abnormal vasculature in tumors from VDR KO mice is associated with increased HIF-1 alpha, VEGF, angiopoietin 1 and PDGF-BB expression

A–D, Tumor extracts were subjected to ELISA analyses for (*A*) HIF-1 alpha, (*B*) VEGF, (*C*) Ang 1 and (*D*) PDGF-BB and the quantification of the growth factors were normalized with total protein. Data shown were from at least 5 tumors per group and statistical analyses were performed using Student's t test. *E*, Representative of 3 experiments showing increased protein expression of VEGF, Ang1 and PDGF-BB in 5 individual tumors from KO mice compared to WT using Western blot analysis. No significant change in the expression of the respective receptors in both groups. *HIF1*, hypoxia-induced factor; *VEGF*, vascular endothelial growth factor; *ANG1*, angiopoeitin-1; *PDGF-BB*, platelet-derived growth factor-BB; *PDGFR*, platelet-derived growth factor receptor.

Table 1

Calcitriol treatment induces G_0-G_1 cell cycle arrest in TDEC expressing VDR

PI staining using flow cytometry was performed with 48 hours vehicle or 10 nM calcitriol treated-TDEC from VDR WT and KO mice. Representative results of three independent experiments are shown.

	WT			KO		
	G_1	S	G_2	G_1	S	G_2
vehicle	45.5	53.1	1.4	42.3	49.5	8.2
10 nM calcitriol	76.9	23.1	0	36.2	50.0	13.8

Cancer Res. Author manuscript; available in PMC 2010 February 01.

Table 2

Tumor vessels in VDR KO mice were enlarged with lower pericyte coverage

Vessel lumen size, % vessel area/field and vessel number/field in tumors were quantified from sections stained with endothelial marker CD31. Pericyte coverage or % SMA was calculated from the overlapping area of CD31 and pericyte marker α-SMA to the total CD31 positive area in each field.

	vessel lumen area (μm)	% vessel area per field	vessel number per field	% SMA positive
WT	271.2 ± 440 (n=5)	0.92 ± 0.87 (n=5)	40.6 ± 15.7 (n=5)	38.9 ± 22.9 (n=5)
KO	3061.6 ± 5081 (n=5) †	23.5 ± 6.5 (n=5) †	41.8 ± 16.6 (n=5)	11 ± 16.8 (n=5) †

n, number of animals;

† $P < 0.001$, compared to WT (Student's t test).